

Earthquake and post-earthquake fire performance of a mid-rise cold-formed steel framed building

Tara Hutchinson, Xiang Wang, Gil Hegemier¹, Brian Meacham, Praveen Kamath², Fernando Sesma³ and Kelly Holcomb⁴

¹*University of California, San Diego, La Jolla, CA*

²*Worcester Polytechnic Institute, Worcester, MA*

³*California Expanded Metals Co. (CEMCO), City of Industry, CA*

⁴*Sure-Board/Intermat, Inc., CA*

Abstract

A unique research collaboration between academia, government, and industry was formed to contribute to understanding the earthquake and post-earthquake fire behavior of mid-rise cold-formed steel wall-braced buildings. Led by the University of California, San Diego (UCSD), with partnerships from Worcester Polytechnic Institute (WPI), government and state agencies, and more than 15 industry sponsors, the centerpiece of this project involved full-scale earthquake and fire testing of a full-scale six-story CFS wall braced building. The test building was constructed on the world's largest outdoor shake table, the Large High Performance Outdoor Shake Table (LHPOST) at UCSD. Within a three-week test program, the building was subjected to seven earthquake tests of increasing motion intensity. Earthquake motions were scaled to impose service, design, and maximum credible earthquake (MCE) demands onto the test building. Subsequently, live fire tests were conducted on the earthquake-damaged building at two select floors. Finally, for the first time, the test building was subjected two post-fire earthquake tests, including a low-amplitude 'aftershock' and an extreme near-fault target MCE-scaled motion. In addition, low-amplitude white noise and ambient vibration data were collected during construction and seismic testing phases to support identification of the dynamic state of the building system. This paper will offer an overview of the earthquake and post-earthquake fire test program and its key findings and implications to design and construction practices.

Introduction

Growth in the use of cold-formed steel (CFS) framed construction has been substantial in recent years, perhaps most notably in high seismic regions in the western United States. Structural systems of this kind consist of repetitively framed light-gauge steel members (e.g., studs, tracks, joists)

attached with sheathing materials (e.g., wood, sheet steel) to form wall-braced component. CFS-framed structures can offer lower installation and maintenance costs than other structural types, particularly when erected with prefabricated assemblies. They are also durable, formed of an inherently ductile material of consistent behavior, lightweight, and manufactured from recycled materials. Compared to other lightweight framing solutions, CFS is non-combustible, an important basic characteristic to minimize fire spread. While these lightweight systems provide the potential to support the need for resilient and sustainable housing, the state of understanding regarding their structural behavior in response to extreme events, in particular earthquakes and ensuing hazards, remains relatively limited.

Previous Work

In the past few decades, a number of experimental investigations have been devoted to advancing understanding regarding the seismic response of CFS-framed shear wall components. The work conducted by Serrette et al. (1997) represents one of the first efforts of its kind in North America to study the seismic response of CFS-framed shear walls. This effort largely formed the initial basis for codified design of CFS systems (e.g., AISI (2007, 2013)). Rogers and colleagues extended their research to investigate CFS wall behavior with varied sheathing materials or framing details (Branston et al. 2006). Their experimental studies included pseudo-static tests of CFS-framed steel strap shear walls (Al-Kharat and Rogers, 2007) and steel-sheet shear walls (Balh et al., 2014), as well as pseudo-dynamic tests of two-story steel-sheet shear wall assemblies (Shamim et al. 2013). In addition, recent experimental studies involve testing of CFS shear walls sheathed with sheet steel (Yu, 2010) or oriented strand board (OSB) panels (Liu et al., 2014). Similar research has occurred outside of North America, including pseudo-static testing of wood-sheathed CFS shear wall tests by Fülöp and

Dubina (2004) and Landolfo et al. (2006) and fastener tests by Fiorino et al. (2007). In contrast, there is a paucity of data regarding the seismic response of CFS-framed buildings configured in their system-level arrangement (whole building tests). The shake table testing of a low-rise (two-story) CFS-framed building within the NSF-supported NEES-CFS program (Peterman et al., 2016a and 2016b) represents the first and only system-level CFS-framed building test in the North America.

Scope of this Project

To address the need for understanding the earthquake and post-earthquake fire behavior of mid-rise CFS-framed buildings, a unique multidisciplinary test project was conducted on the Large High Performance Outdoor Shake Table (LHPOST) at University of California, San Diego (UCSD) between April and July 2016. Central to this research is the system-level earthquake and live fire testing of a full-scale six-story CFS wall braced building. In a three-week test program, the building was subjected to seven earthquake tests of increasing motion intensity. Earthquake motions were scaled to impose service, design, and maximum credible earthquake (MCE) demands onto the test building. Subsequently, live fire tests were conducted on the earthquake-damaged building at two select floors. Finally, the test building was subjected to two post-fire earthquake tests, including a low-amplitude ‘aftershock’ and an extreme near-fault target MCE intensity motion.

Test Building Design

A full-scale cold-formed steel (CFS) test building was designed and erected on the large, high-performance outdoor shake table at UC San Diego (NHERI@UC San Diego). For the purposes of design, this six-story CFS framed test building (Figure 1) was assumed to be located in a high seismic region near downtown Los Angeles, with its design basis complying with current code provisions within ASCE 7-10 (ASCE, 2010), AISI S100 (AISI, 2012), and AISI S213 (AISI, 2007). For simplicity, a uniform plan with dimension of 10.4 m × 7.3 m (34 ft × 24 ft) at each floor was adopted, allowing the specimen to occupy almost the entire 12.2 m × 7.6 m (40 ft × 25 ft) shake table footprint. The total height of the building was 19.2 m above the shake table platen (a floor-to-floor height of 3.1 m (10 ft) for all stories and a 1.2 m-tall (4 ft tall) parapet on the roof perimeter). The seismic design considered uniformly distributed dead and live loads of 1.5 kN/m² (32 psf) and 1.9 kN/m² (40 psf) at each floor, with the exception of an assumed live load on the roof of 1.0 kN/m² (20 psf). Consequently, the effective seismic design weight of the test building was assumed as 1420 kN (320 kips). According to ASCE 7-10 (ASCE, 2010), the CFS wall braced building was designed with a response modification factor R

of 6.5, an overstrength factor Ω of 3.0, and a deflection amplification factor C_d of 4.0. The code-based fundamental period of the test building T was determined as 0.43 sec considering a total building height of 18.3 m (60 ft) excluding the parapets. The base shear coefficient C_s of the test building was consequently determined as 0.236 and resulted in an effective seismic design base shear V_b of 334 kN (75 kips). It is noted that the weight of the building was directly determined using measurements recorded during the nine earthquake tests. From these measurements, the average building weight, including its nonstructural components was 1160 kN (260 kips). While this was ~260 kN (60 kips) lower than that used for the design, this was anticipated and accounts for the reduction of live loads (reduction factor of ~0.6) in the event of an earthquake. The estimated maximum inelastic story drift of the building was ~1.0% (with a deflection amplification factor C_d of 4.0, which was lower than the allowable story drift of 2.0% as prescribed in ASCE 7-10 (ASCE, 2010).

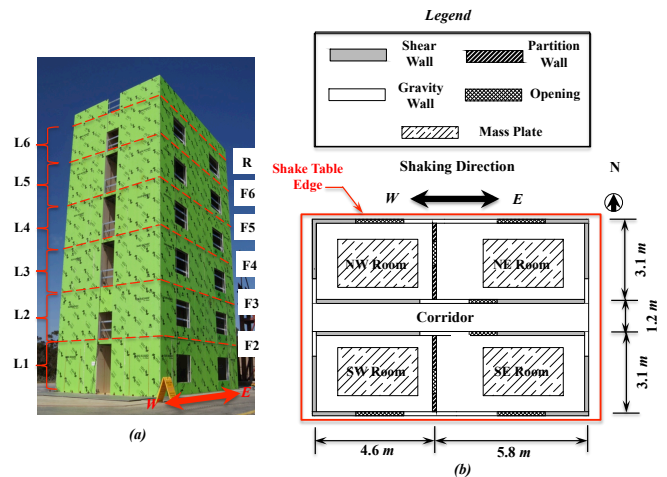


Figure 1. Test building: (a) isometric photograph, and (b) schematic building plan layout (typical of floor 2 to 6, note that floor 1 is identical sans the transverse partition walls).

In terms of layout, as shown in Figure 1b, the building had a symmetric floor plan with a 1.2 m (4 ft) wide corridor oriented along the longitudinal centerline and a room at each quadrant of the building. Two transverse partition walls were located 0.6 m (2 ft) west of the transverse centerline (level 2 through level 6), each separating the two rooms on the same side of the corridor. It should be noted that no partition walls were installed at the first level to retain simplicity in attachment to the shake table. The exterior wall layout of the building resulted in four partial-height window openings (one at each room) and two full-height corridor openings (at each end of the corridor) at each level (Figure 1a). Dropped (partial-height) soffits were constructed on the corridor openings at the level 2 and level 6 to attain the anticipated ventilation condition for the fire tests. To account for the live

loads and the weight of certain architectural features excluded from the construction (e.g., flooring, exterior façade finishing), four mass plates were installed on the floor diaphragm at each floor from the second floor through the roof (Figure 1b). Each mass plate had a dimension of 3.0 m × 1.8 m (10 ft × 6 ft) and had a weight of ~16.5 kN (3.7 kips).

CFS Component Details and Construction

The test building was detailed to carry lateral seismic loading using prefabricated repetitively framed CFS-floors and walls with shear load resistance provided via steel sheathing. As illustrated in Figure 1b, two longitudinal shear walls were placed along each (east and west) end of the corridor, with an associated wall length of 4.0 m (13 ft) for the walls at the west end and 3.3 m (11 ft). In addition, short shear walls with a length of ~1.6 m (5'-4") in the longitudinal direction and ~2.1 m (7 ft) in the transverse direction were placed at the four corners of the building. The total shear wall length per floor was 21.3 m (70 ft) in the longitudinal (shaking) direction and 8.6 m (28 ft) in the transverse direction. It is noted that the corridor shear walls were designed as the primary lateral load resisting elements in the direction of shaking, while the corner shear walls were assumed to resist transverse and torsion loads during the tests.

The shear walls were framed using standard framing members (e.g., studs, tracks; Figure 2). Sheathing materials utilized load-resisting structural panels on the exterior (or corridor) side and 16 mm (5/8") thick regular gypsum boards on the room side. The structural panels were fabricated using 16 mm (5/8") thick gypsum boards (or) bonded with a layer of 0.686 mm (0.027") thick (22 ga.) sheet steel to provide shear resistance to the shear wall assemblies. For the corridor shear walls, vertical studs utilized 600S200-68 at 610 mm (24") o.c at the first level and 600S200-54 at 610 mm (24") o.c at all remaining levels. The (top and bottom) tracks were consistently constructed using 600T200-54, with the exception of the first level bottom tracks that used 600T200-97. In addition, the chord studs (in a double stud pattern) at the edge of the door and opening windows were constructed using 600S200-68. The structural panels of the corridor walls were attached to framing using #8 self-tapping metal screws at 406 mm (16") o.c in field and varying boundary (edge) spacing of: 76 mm (3") o.c. for the lower three levels, 102 mm (4") for level 4, and 152 mm (6") o.c for the upper two levels. It is also important to note that corridor and corner shear walls contained a pair of tie-down subassemblies (consisting of tie rods and compression posts) as part of the building tie-down system.

The floor and roof diaphragms of the test building were also constructed using a prefabricated steel member framing system, however individual edges of the diaphragm were

attached using a ledger framing system. Namely, they were connected to the vertical structural system by attaching the diaphragm joists to the flange of the wall studs via a combination of rim track and clip angle solution (e.g. Figure 3). The diaphragm joists were oriented perpendicular to the longitudinal direction of the building (direction of shaking), resulting in a clear span length of ~2.9 m (9'-6") for the room span and ~1.1 m (3'-6") for the corridor span.

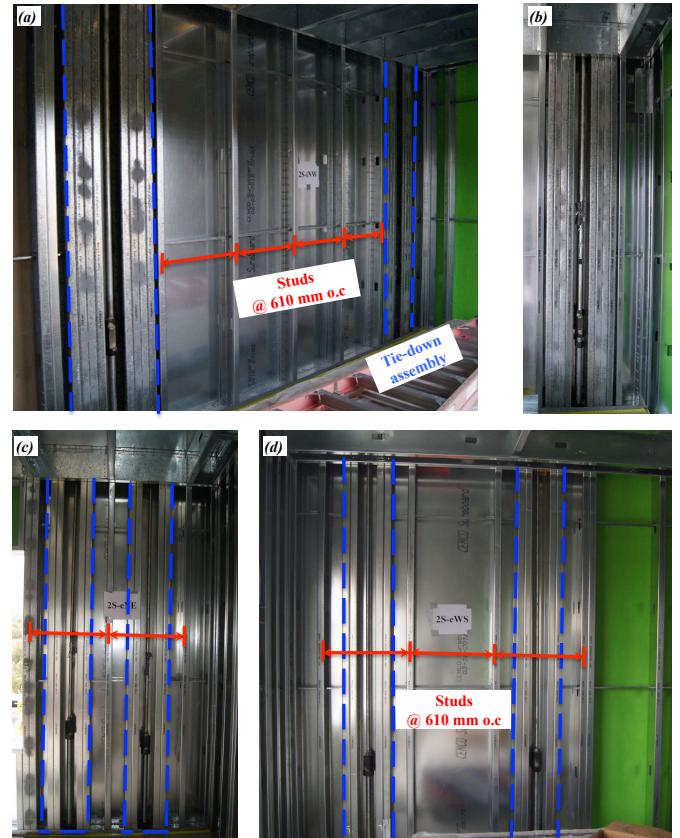


Figure 2. Example of shear wall framing (level 2): (a) corridor wall, (b) corridor wall tie-down subassembly, (c) longitudinal corner wall, and (d) transverse corner wall (all photos view from room side with gypsum removed).

Irrespective of the span length, the diaphragm framing was consistently constructed using 1000S200-54 at 610 mm (24") o.c for the joists (aligned with the vertical wall studs) and 1000T200-54 for the rim tracks at all floors of the building including the roof (Figure 3). The joist was connected to the rim track using 7-1/2"x2"x2" angles with (5) #10 metal screws vertically spaced over the flange. It is also noted that both the diaphragms contained mid-span blocking or bracing to enhance their shear capacity. The floor sheathing consisted of fiber reinforced cement boards bonded with a layer of 0.838 mm (0.033") thick (20 ga.) sheet steel. The thickness of cement boards was 14 mm (9/16") at floor 2 through 6 and 11

mm (7/16") at the roof. The floor sheathing was attached to the upsides of the joists and rim tracks using #8 drywall screws at 152 mm (6") o.c both in field and on boundary. In addition, the underside of floor 3 and roof was sheathed with 16 mm (5/8") thick regular gypsum panels to provide a compartmentalized fire-testing environment. The gypsum panels were attached to the underside of the joists and rim tracks using #8 drywall screws at 152 mm (6") o.c both in field and on boundary.

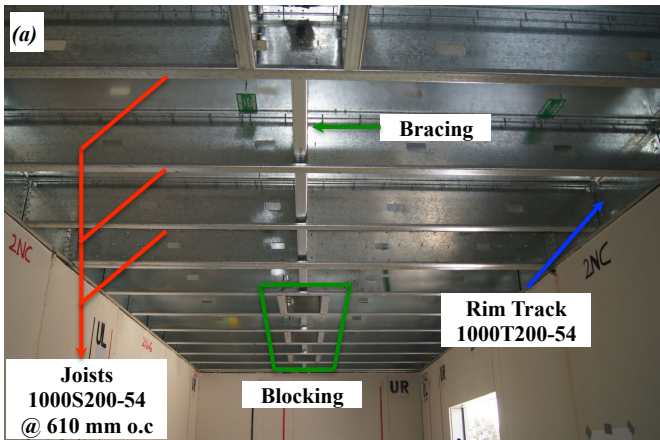


Figure 3. Example of room span floor diaphragm (view from room below).

Test Building Construction

Construction of the test building commenced in April 15, 2016 with the shake table platen tie-down installation. A total of 80 large-diameter rods were used to attach the first-level bottom tracks to the table at a space at 0.6 m (2 ft) along the bottom tracks (Figure 4a). Subsequently, the first-story wall system was fabricated in-situ for a total of four days (Figure 4b). Following completion of the first-story wall system, the building construction significantly expedited as a result of the highly efficient panelized construction (Figure 4c-d). Construction of the upper levels progressed at a rate of one level per day. The erection of the building skeleton was completed on April 27, 2016 (total of nine construction days; Figure 4d). Figure 4e shows the layout of the mass plates (one at each quadrant) at the roof of the building, which represented the typical mass configuration of the roof and all other floors during the earthquake tests. These plates were installed on and attached to the diaphragms in conjunction with building erection.



Figure 4. Construction of the test building: (a) building tie-down system (April 16, 2016), (b) in-situ installation of first-story wall system (April 19, 2016), (c) installation of a prefabricated wall panel at the third story (April 23, 2016), (d) completion of building skeleton erection (hoisting the final piece of roof panel) (April 27, 2016), and (e) roof mass plate layout prior to the earthquake tests (June 10, 2016).

It is noted that, in conjunction with building erection, a temporary platform stair tower was installed on the northeast side of the building to support access to the test building. This stair tower was detached from the building during all earthquake and low-amplitude white noise tests, however it was reconnected to the building at the completion of a test sequence on each test day and provided access for the inspection activities.

Interior construction commenced immediately following the completion of the building erection. Activities related to interior construction included: 1) installation of interior gypsum panels (structural walls, nonstructural walls, and ceiling), 2) installation of interior partition walls, 3) door installation, and 4) appliance installation (on the first and sixth floors only). These activities spanned about an entire month and the interior installation was completed at the beginning of June 2016. Interested readers are referred to the video links ^[1,2] of the building construction and demolition time lapses.

¹ Construction time lapse available at https://www.youtube.com/watch?v=IFq7Nv_020c.

² Demolition time lapse available at <https://www.youtube.com/watch?v=EIOiksCJUKM>.

Test Protocol

The three-week test program consisted of a sequence of nine earthquake tests and six fire tests between June 13 and July 1, 2016. During the first week (pre-fire test phase), the building was subjected to seven earthquakes with increasing input motion intensity in three test days (June 13, 15, and 17, 2016). Subsequently, live fire tests were conducted on the earthquake-damaged building at the second and sixth levels of the building across a period of three consecutive days (June 27–29, 2016). The test program concluded with two post-fire earthquake tests on the final test day at the end of the third week (July 1, 2016). To complement the earthquake and fire test sequence, low-amplitude vibration tests in the form of white noise and tire (shock) tests as well as ambient vibration tests were conducted throughout the construction and test phase. It is noted that all of the earthquake and white noise test motions were applied in the east-west direction using the single-axis shake table, whose axis coincided with the longitudinal axis of the building. In the present paper, we focus on primarily the earthquake test sequence, both pre- and post-fire tests.

Earthquake Motions

Earthquake motions were selected for the shake table testing considering the following key objectives: (a) inclusion of multiple intensity levels in the seismic test protocol, (2) design level event representative of strong earthquakes in California, and (3) inclusion of earthquake events with a wide variety of motion characteristics (e.g., near-fault pulse effect, strong durations). Guided by these selection criteria, four test motions from three earthquake events were chosen and subsequently scaled to achieve service, design and maximum credible hazard scenarios. The characteristics of the seed (unscaled) test motions are summarized in the acceleration histories, pseudo-acceleration and displacement spectra in Figure 5. Note that three seed motions were selected from earthquake events in California (short names of: CNP196 and RRS228 from the 1994 $M_w=6.7$ Northridge earthquake, while RIO 360 is from the 1992 $M_w=7.0$ Cape Mendocino earthquake). The remaining motion (CUREW) is from the 2010 $M_w=8.8$ Maule earthquake in Chile, a large-magnitude subduction event. Notably, the strong motion duration of CUREW was significantly longer than the other three records. Furthermore, RRS228 differed fundamentally from the other three records in the spectral characteristics, as it contains an appreciable velocity pulse and wide spectral peak in the period range between 0.5 and 1 second (even larger than its short period spectral accelerations), while the pseudo-acceleration spectra of other three motions drops considerably when the period exceeds ~ 0.5 second. Motion RRS was recorded near to the fault, and contained a long period velocity pulse at around 1.2 second.

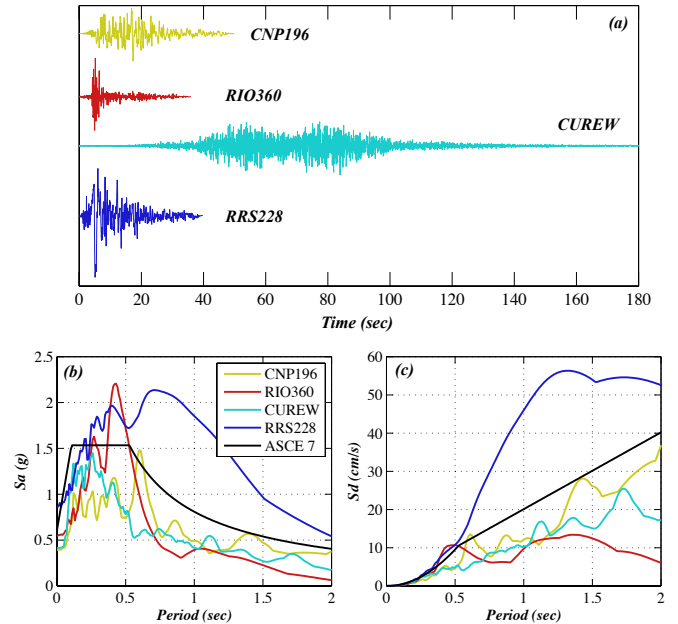
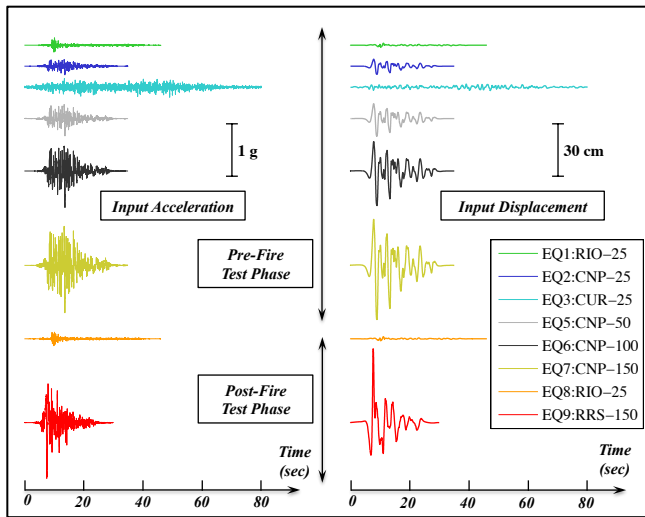


Figure 5. Seed motions: (a) acceleration time histories, (b) pseudo-acceleration spectra ($\zeta = 5\%$), and (c) displacement spectra ($\zeta = 5\%$).

Scaling of these seed motions was applied to define a testing sequence which would invoke a range of increasing intensity performance states in the structure, namely serviceability, near and at design, and maximum credible. The final acceleration and displacement time histories of the achieved input earthquake motions are shown in Figure 6a. The 5% damped elastic response spectra of the achieved motions are shown in Figure 6b. It is noted that the strong motion duration of all input motions were between 10 and 20 seconds, with the exception of the subduction event (EQ3) that had a strong duration of over 50 seconds. It is also notable that the first seven earthquake motions (pre-fire test sequence) were applied at increasing intensity to progressively damage the building, as the peak input accelerations of the motions increased from 0.15 g to 0.9 g and the spectral accelerations at the fundamental period of the test building $S_a(T_1, 5\%)$ increased from 0.3 g to 2.0 g. The last two test motions (post-fire test sequence) were intended to represent a service-level aftershock event (EQ8 – a replicate of the motion EQ1) and a near-fault extreme earthquake event (EQ9) with a peak input acceleration above 1.0 g.



During the earthquake test phase, the seismic response of the test building was monitored with a dense array of analog sensors consisting of accelerometers, displacement transducers (string potentiometers and linear potentiometers), and strain gauges. Table 1 summarizes the five different types of analog sensors and the corresponding measured responses, while Figure 7 offers a sample of a typical floor accelerometer layout. With the exception of the Kinometrics accelerometers that collected data using a standalone data acquisition system at a sampling frequency of 200 Hz, all remaining analog sensors were connected to a multi-node distributed data acquisition system and set to sample at a frequency of 240 Hz.

Table 1. Summary of analog sensors and their location.

Sensor type	Type and locations of measurements
Accelerometer (MEMS)	Floor accelerations on all floors; equipment accelerations at floor 6
Accelerometer (Kinometrics)	Floor accelerations at floor 2, 4, 6, and roof
String potentiometer	Shear wall distortion at levels 1, 2, and 4; floor displacements at lower 4 floors
Linear potentiometer	Shear wall uplift at levels 1, 2, and 4; floor joist displacements at floor 2
Strain gage	Tension rod strains at levels 1, 2, and 4, compression post strains at level 1

Figure 6. (top) acceleration and displacement time histories of the achieved input motions and (bottom) elastic response spectra of achieved motions ($\zeta = 5\%$): (a) pseudo-acceleration spectra, and (b) displacement spectra.

Specimen Instrumentation

The building was outfitted with more than 250 analog sensors, a Global Positioning System (GPS) system, and an array of more than 40 digital video cameras to record the behavior of the structural components and building in the earthquake tests. Between the two earthquake test phases, thermocouples were installed in various locations of the fire test compartments. Sacrificial video cameras were also installed to collect visual data regarding smoke or fire spread. In addition, remote sensing systems, such as unmanned aerial vehicles (UAVs) and light ranging and detection (LiDAR) systems, were employed to collect various data during the construction and testing. In addition, a building reference system was developed to facilitate building interior and exterior documentation during construction and testing phase. The analog instrumentation is briefly discussed in this section, with particular emphasis on those sensors utilized to characterize the specimen's response to the earthquake test sequence.

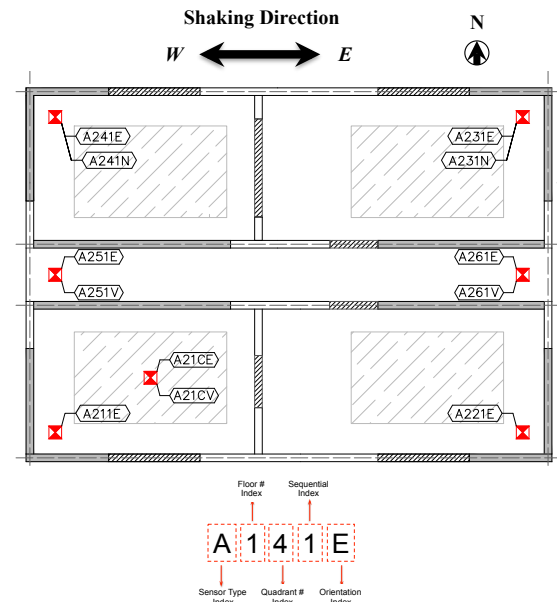


Figure 7. Typical layout of accelerometers (plan view) at a floor level and notation definition (bottom).

Dynamic Characteristics of the Test Building

Low-amplitude vibration tests (e.g., white noise base excitation tests, ambient vibration tests, and shock tests) were conducted at various stages during the test program, including 11 white noise tests during the pre-test (construction) phase and 20 white noise tests during the test phase. A comprehensive system identification study is then conducted to understand the evolution of the modal characteristics (e.g., natural periods, damping ratios, and mode shapes) of the test building at the various stages of the test program using acceleration data collected from the low-amplitude vibration tests.

Figure 8 offers a summary of the first two fundamental periods and damping ratios as a function of state. Although determined using white noise conducted between test motions, these plots nominally articulate the buildings dynamic state throughout the various test phases; from service, design, MCE, fire, and post-fire earthquake demands. Naturally the period elongates under increasing seismic demands, with an initial fundamental longitudinal period of $T_1 \sim 0.3s$ and a near doubling in fundamental period following the DE (EQ6), and a near three-fold increase in $T_1 \sim 0.85s$ following the MCE (EQ7) test. Correspondingly, larger damping is available once the system state is inelastic (increasing from $\sim 9-10\%$ (SLE) to $>20\%$ after the DE). Notably however, very little change in fundamental period is observed following the fire tests, though a substantive drop in damping is realized (between S7 and S8); this reduction in damping can be anticipated to lead to much larger seismic demands during the post-fire earthquake tests, however is sensitive to the low amplitude of white noise imposed.

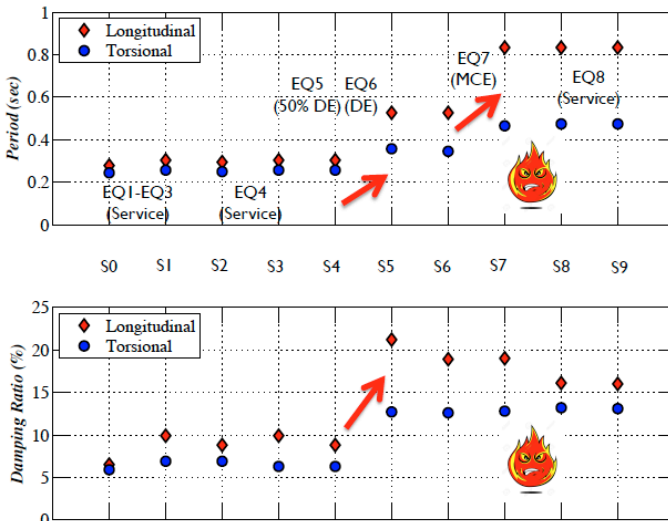


Figure 8. First two fundamental periods and damping ratios as a function of state (S0-S9) of the test building.

Earthquake Test Results

Two distinct phases of earthquake testing were conducted during this program. In this paper, these are subdivided into the pre-fire and post-fire earthquake tests measured and physical observation results.

Measured Response: Pre-Fire Tests

This section focuses on presenting the test results of the system-level building response during the pre-fire earthquake test sequence, which include the building global response (e.g., floor accelerations, interstory drifts, and residual displacements, story shear forces). In particular, a comparison amongst the response under the service level (SLE) [EQ2], design event (DE) [EQ6], and maximum credible event (MCE) [EQ7] are emphasized. In addition, the physical damage of the test building and its nonstructural systems (e.g., partition walls, appliances, and doors) during the pre-fire earthquake test sequence is discussed.

Floor Acceleration Demands: Figure 9 and 10 present the absolute floor accelerations at the center of the building from floor 1 to the roof during EQ2:CNP-25 (SLE) and EQ7:CNP-150 (MCE), respectively. In these figures, each row contains the floor accelerations in the three directions (longitudinal, transverse, and torsional) at a specific floor. It is noted that the units of the torsional accelerations (rad/sec^2) differs from that of the horizontal accelerations (g). The annotated text in each plot denotes the floor number and orientation of the time history response (e.g., 2-T indicates the transverse acceleration at floor 2). The color circles represent the time instances of the maximum (red) and minimum (green) responses to facilitate comparing the phase correlation of the responses at different floors or levels. These histories consistently demonstrate the increasing acceleration with height in the building, as well as the significant increase in floor acceleration amplitude with increasing event intensity. To synthesize these histories, Figure 11 presents the peak floor acceleration distribution along the height of the building in the complete pre-fire earthquake test sequence. The peak accelerations correspond to those associated with the center of each floor. Sans test EQ7, the longitudinal floor accelerations increases monotonically up the height of the building with the largest values at the roof during each test. While relatively small during the service level earthquakes ($<0.5g$), the longitudinal peak roof accelerations achieved about $2g$ during the design event (EQ6) and exceeded $3.5g$ during the MCE event (EQ7). The transverse accelerations remained less than 10% of its longitudinal counterparts in all pre-fire tests Figure 11a). To facilitate the torsional and longitudinal acceleration comparisons (for consistency in units), the torsional accelerations are multiplied by the building width to represent the translational accelerations

induced by the torsional motion. By comparing Figure 11a and c, the torsion-induced accelerations in the longitudinal direction are about 20% – 30% that at the center of the floor up to the design event (EQ6), however, were as large as 60% at the roof during the MCE event (EQ7).

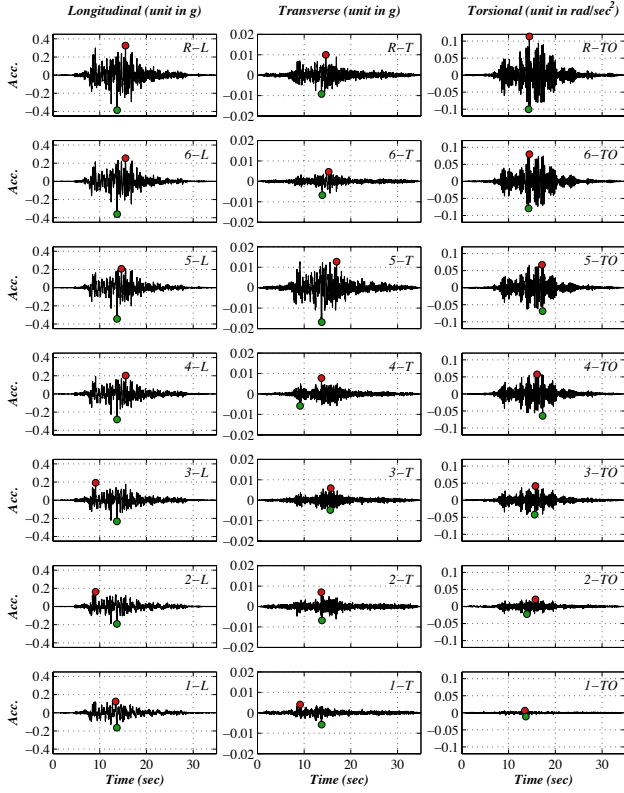


Figure 9. Floor accelerations – SLE (EQ2:CNP-25).

Drift Demands: The interstory drift ratios (IDRs) at the corners at all six levels during the SLE and MCE tests are summarized in Figures 12 and 13. These figures contain the longitudinal and transverse IDRs at the center of all levels as well as the interstory rotations (IRs). It is noted that the unit of IR (rad) differs from that of the longitudinal and transverse IDRs (%). These histories demonstrate that early in the test sequence (SLE), the specimen observed relatively uniform interstory drift demands, with height; however, upon increased motion intensity (Figure 13 – MCE), larger interstory drift demands were concentrated in the mid-height of the building. A synthesis of the peak IDRs (PIDR) for all pre-fire test motions is provided in Figure 14. The PIDRs correspond to those associated with the center of each floor. These distributions indicate that the largest longitudinal PIDRs occurred at the mid level (level 4) during all pre-fire tests. While relatively small in amplitude during the service level earthquakes (PIDRs < 0.1%), the longitudinal PIDRs achieved about 1% during the design event (EQ6) and exceeded 1.5% during the MCE event (EQ7). Notably, development of the intended wall panel yielding mechanism

is consistently observed in wall-component cyclic tests (see e.g. Hoehler et al., 2017). The transverse PIDRs at the upper three levels appeared considerably larger than those at the lower levels, while the PIR consistently achieved the largest values at the top level (level 6) during all tests.

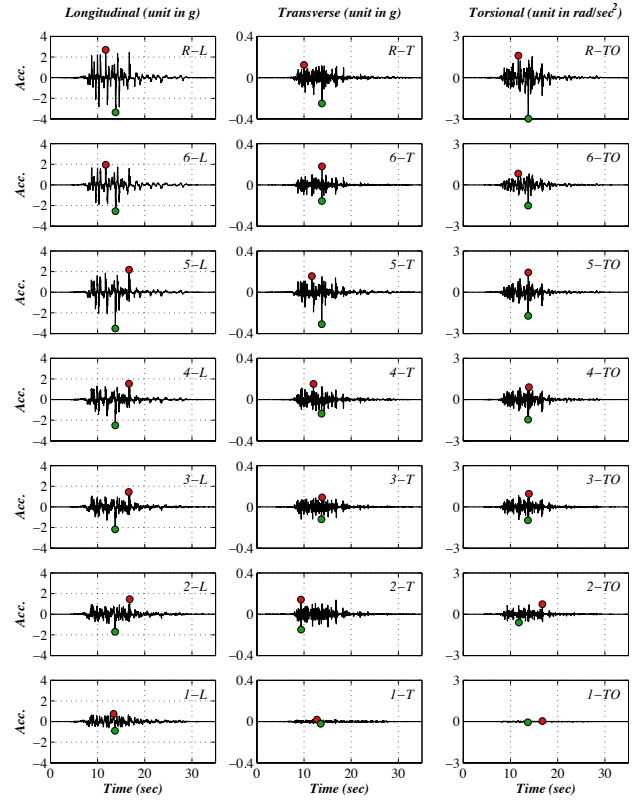


Figure 10. Floor accelerations – MCE (EQ7:CNP-150).

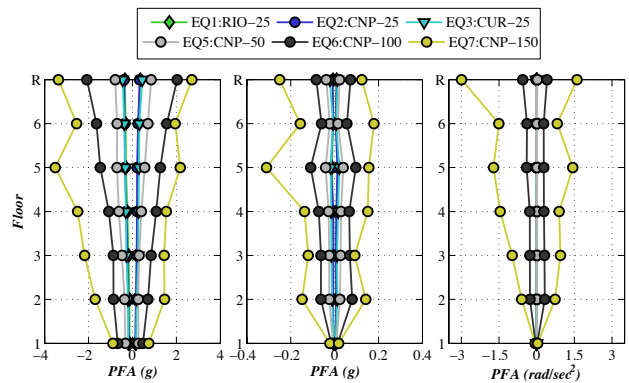


Figure 11. Peak floor accelerations in the pre-fire earthquake tests: (a) longitudinal, (b) transverse, and (c) torsional.

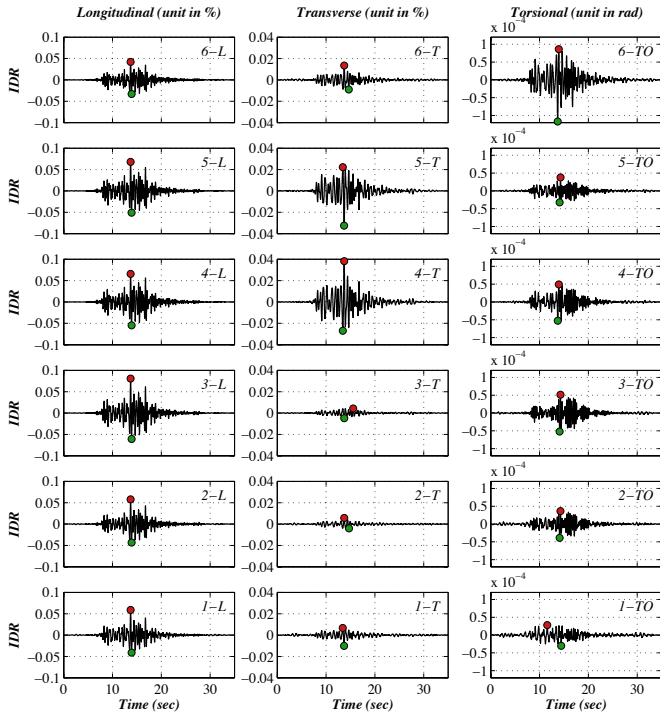


Figure 12. Interstory drift ratios – SLE (EQ2:CNP-25).

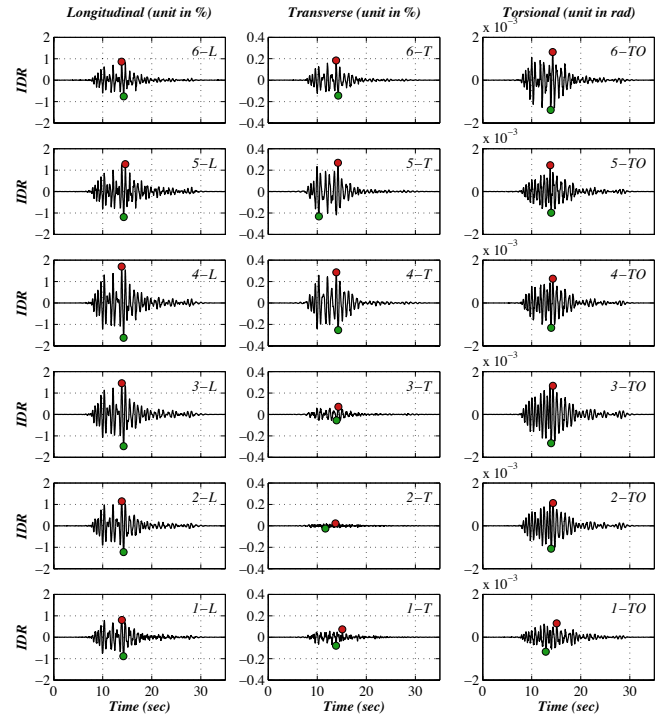


Figure 13. Interstory drift ratios – MCE (EQ7:CNP-150).

Figure 15 presents the peak roof drift ratio (PRDR) in the longitudinal direction during all tests conducted pre-fire. The RDR is defined as the ratio between the roof displacement relative to that of the table platen divided by the total building height (excluding the parapets). It is noted that the absolute roof displacement was obtained using direct measurement from the GPS system mounted on the roof (center station), while the table absolute displacement was measured by the string potentiometer at the first floor (table platen). This plot further demonstrates that longitudinal RDR was relatively small ($< 0.1\%$) during the service level events (EQ1-EQ3) but increased to about 0.8% for the design event (EQ6) and attained about 1.5% for the MCE event (EQ7). In addition, the residual roof displacement (or residual RDR) was also determined using the direct GPS measurements at the roof (center station). During the pre-fire test phase, the building observed no apparent residual roof displacements up to the design event (EQ6), with a calculated residual displacement at the roof less than 0.5 cm ($<$ than the noise level of GPS measurements). The roof residual displacement became slightly larger (~ 1.5 cm) for the MCE event (EQ7), which corresponds to only a roof drift ratio of $\sim 0.1\%$.

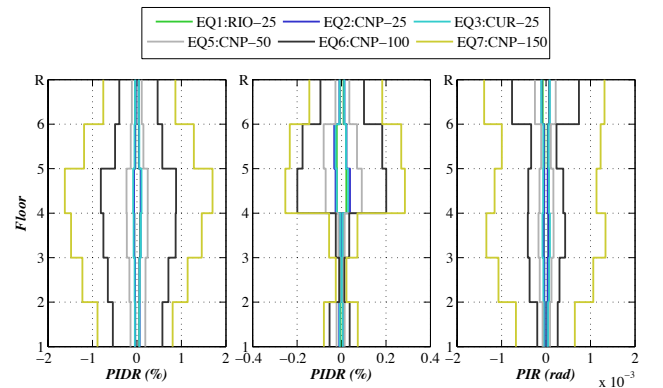


Figure 14. Measured peak interstory drift ratios (a) longitudinal, (b) transverse, and (c) peak interstory rotation in the pre-fire earthquake test sequence.

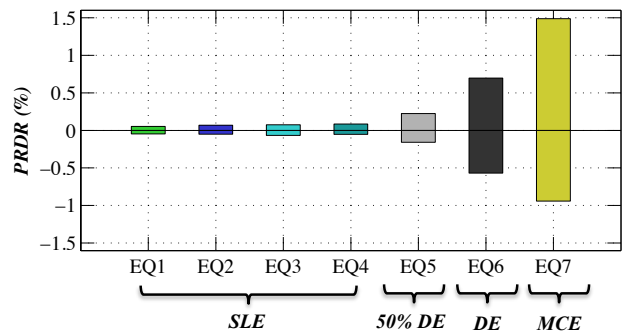


Figure 15. Peak roof drift ratios measured during the pre-fire earthquake tests.

Figure 16 presents the normalized peak base shear versus peak roof drift ratio (PRDR) response during the pre-fire test sequence. As clearly indicated, the building responded almost elastically up to the 50% design event (EQ5). This is consistent with the physical observations during testing, where little to no damage was noted. Although the base shear increased in proportion with the motion intensity for the design event (EQ6), the roof drift ratio increased three-fold between the 50% design event (EQ5) and the design event (EQ6). This is indicative of the onset of nonlinear deformation of the test building. The roof drift ratio continued to increase during the MCE event (EQ7), while the base shear demand remained comparable to that in the previous test, indicating the saturation of system lateral strength.

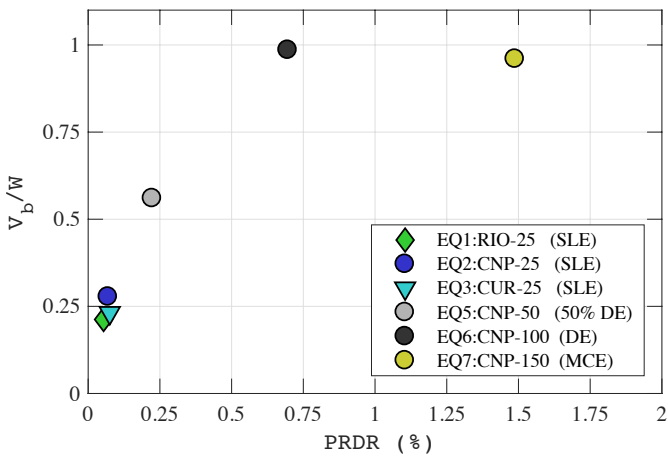


Figure 16. Peak normalized base shear forces versus peak roof drift ratio (pre-fire earthquake tests)

Shear Force, Story Stiffness, and Period Estimates: The shear force versus interstory drift ratio hysteretic responses during one of the service level events (EQ2: CNP-25) is shown in Figure 17. It is noted that the story shear force accounts for the contributions of all the (corridor and corner) shear walls and gravity walls (even their contributions are not considered as significant) at the specific level, while the interstory drift ratio is taken as that associated to the floor centers. These plots demonstrate that the response of the lateral force resisting system was essentially elastic at all levels during the service level event (EQ2) with the story shear force achieving ~300 kN at the lower two levels. Due to the increased motion intensity during the design event (EQ6) and MCE event (EQ7), the hysteretic response exhibited significant pinching effects that are representative of the nonlinear behavior of CFS wall systems (see Wang et al., 2017a for additional results). Since, the story shear force versus interstory drift response remained essentially linear during the service level test sequence, the story stiffness of the building during these service level tests can be estimated by fitting a straight line through the response. This is determined using least square

regression on the measured response associated with very small drifts (note that < 0.01% IDR are excluded). Provided the estimated story stiffness over the building height, the building dynamic characteristics (fundamental period and the effective modal mass) can be further determined using eigenvalue analysis of a simplified shear beam model with the building mass lumped at the floor level.

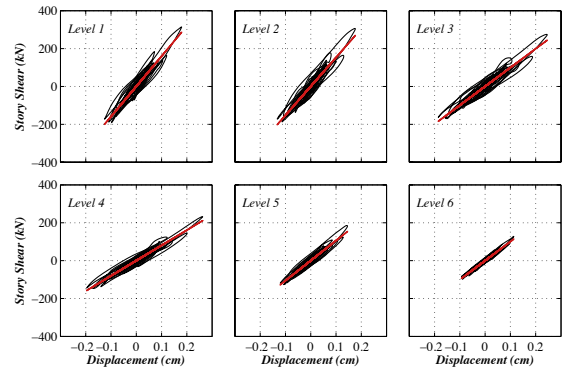


Figure 17. Story shear versus story displacement response, including idealized linearization (red) – SLE (EQ2:CNP-25).

Figure 18 summarizes the estimated story stiffness during all three service level tests (EQ1 – EQ3) and the story stiffness of all levels normalized by the stiffness of level 1. This summary shows that the story stiffness at all levels reduced slightly during the service level tests, however the reductions were less than 20% of their initial values. Notably, while the story stiffness of level 1 and 2 remained comparable, the story stiffness at the upper levels were only 50% and 60% those of the lower two levels (Figure 18b). This is explained the fact that the largest interstory drifts consistently occurred at the middle of the building during all pre-fire tests. Since the framing studs and screw spacing of the shear walls at the lower three levels remained almost identical, the distinctive differences in the story stiffness between the lower two levels and level 3 are likely attributed to the tie-rod system details (compression posts and tie-rod diameter).

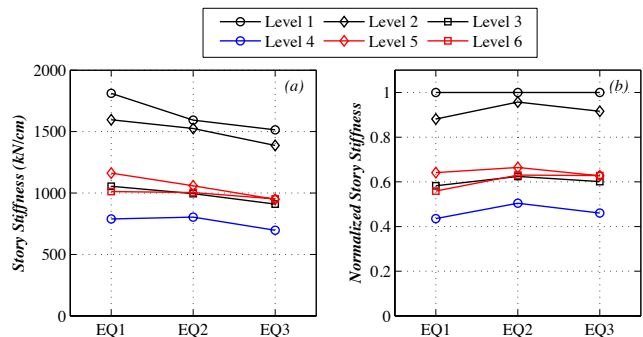


Figure 18 Estimated story stiffness during all SLEs.

Table 2 summarizes the fundamental period of the building (in the direction of shaking) and the effective normalized modal mass during the service level earthquake tests (EQ1 – EQ3); calculated using the story stiffness estimates. As shown in the table, the estimated fundamental period was about 0.3 second with an effective modal mass of about 80% of the total mass of the building during the three service level tests. The estimated periods are consistent with those identified using the white noise tests, which ranged between 0.26 ~ 0.29 second (the small discrepancies of the periods are attributed to the amplitude differences between the white noise excitations and the input earthquake excitations). It is important to note that the estimated fundamental period as identified during the low-amplitude earthquake tests differed notably from (more than 25% smaller than) the code-specified period of 0.43 second as considered in the seismic design.

Table 2. Estimated building fundamental period during the service level earthquake (SLE) tests

Test	T_1 (sec)	M_{eff} (%)
EQ1:RIO-25	0.31	79.7
EQ2:CNP-25	0.32	80.7
EQ3:CUR-25	0.33	80.1

Physical Observations: Pre-Fire Tests

Detailed physical inspection of test building and its nonstructural components was conducted at four different stages throughout the pre-fire earthquake test phase: (1) pre-test inspection (associated with state S0), (2) post-SLE (associated with state S3), (2) post-DE (associated with state S6), and (3) post-MCE (associated with state S7). In addition, rapid inspections were conducted between the tests during the first two test days that involved multiple earthquake tests, although the primary purpose of these inspection was to examine the condition of critical structural components (e.g., mass plate anchorage, tie rod coupler connections).

Due to the low seismic demands during the service level tests at all levels of the test building (PFA < 0.5 g, PIDR < 0.1%), the interior sheathing sustained only a few instances of minor damage (DS-1) in the form of incipient screw withdrawal and localized gypsum crushing at bulging at level 3 and 4 while no visible damage to interior sheathing occurred at all other levels. The extant of sheathing damage, however, was considered inadequate to classify the walls into an appreciable damage state. Damage to the interior sheathing however did continue to develop as the seismic drift demand increased during the 50% design event (EQ5) and design event (EQ6). Screw withdrawal and gypsum crushing of the

corridor shear walls and gravity walls became more pervasive at all levels (except level 6), in particular at the corridor shear wall–gravity wall boundaries as well as the window and door openings (Figure 19a-d). In contrast, damage to the corner shear walls remained minor, as they occurred only in the form of localized gypsum crushing at the corner and formation of gaps between gypsum panels. Since the interior gypsum was mudded and tapped at level 2 and 6 (in preparation for the fire tests), tape cracking or flaking along the panel joints was also observed at these levels. Other ancillary damage was also noted, for example, a punched opening was detected on the gypsum panels at the northeast room at level 6 due to the toppling of a water heater during EQ6 (Figure 19e).



Figure 19. Sheathing damage following the design level test (EQ6): (a) corridor shear wall–gravity wall boundary at level 4 (upper), (b) (a) corridor shear wall–gravity wall boundary at level 4 (lower), (c) pervasive screw withdrawal and corner crushing of gravity wall at level 4, (d) corridor gravity wall boundary crushing at level 2, and (e) a punched opening on the gypsum panel at level 6.

Following the completion of the pre-fire earthquake test sequence, the gypsum panels of the northwest compartment at level 4, which represented the level with the largest drift demand during the pre-fire test sequence, were removed to allow for inspection of the shear wall framing and sheathing steel (Figure 20a). As shown in Figure 20b-d, localized buckling of the sheathing steel was detected at the top of corridor shear wall, while the framing studs and tracks did not sustained apparent damage (Figure 20e). In contrast, the

wall framing and sheathing steel of the corner shear wall in the same compartment sustained no apparent damage. In addition, loosening of the bolts at the floor bearing connections was detected, resulting in very loose tie rods at the end of the pre-fire sequence.



Figure 20. Longitudinal corridor shear wall framing following the pre-fire MCE test (EQ7): (a) wall framing, (b) localized buckling at the top of sheathing steel, (c) and (d) close-up of the localized buckling, (e) bottom track, and (f) loosened bolt of the tie-rod bearing connection.

Measured Response: Post-Fire Tests

This section presents the seismic response of the test building during the post-fire earthquake test sequence, which involved a service-level aftershock event (EQ8:RIO-25) and a near-fault extreme event (EQ9:RRS-150). Results presented herein include the global building responses (e.g., floor accelerations, interstory drifts, and residual displacements). These results are compared with those measured during the pre-fire earthquake tests to characterize the effect of prior earthquake-fire damage on the behavior of the test building. It is noted that the final near-fault extreme event induced significant damage, near collapse, on the building; therefore an important aspect of the subsequent discussion involves documenting the residual, final state of the building.

Comparison of Floor Acceleration and Drift Demands: To facilitate the comparison of seismic behavior of the test building during the pre-fire and post-fire earthquake tests, the peak building responses during the pre-fire and post-fire earthquake tests, including peak floor

accelerations (PFAs), peak inter-story drift ratios (PIDRs), peak roof drift ratios (PRDRs), and residual roof drift ratios (RDR_{res}), are summarized in Table 3. These data immediately articulate the increasing demands (consistent across all quantities) appreciated during the final extreme test (EQ9). Floor-by-floor assessment, in what follows, guides the interpretation of the distribution of these demands during each test and as realized before and after the fire test sequence.

Table 3. Peak building responses during the earthquake tests

Test Motion	PFA (g) (Floor #)	PIDR (%) (Level #)	PRDR (%)	RDR_{res} (%)
EQ1:RIO-25	0.35 (R)	0.08 (L4)	0.05	0.0
EQ2:CNP-25	0.38 (R)	0.09 (L4)	0.07	0.0
EQ3:CUR-25	0.45 (R)	0.10 (L4)	0.08	0.0
EQ4:CNP-25	0.43 (R)	0.10 (L4)	0.09	0.0
EQ5:CNP-50	0.85 (R)	0.24 (L3)	0.19	0.0
EQ6:CNP-100	2.07 (R)	0.89 (L4)	0.70	0.0
EQ7:CNP-150	3.77 (F5)	1.70 (L4)	1.49	0.1
Fire Test Sequence				
EQ8:RIO-25	0.16 (R)	0.17 (L3)	0.12	0.0
EQ9:RRS-150	4.43 (F5)	12.2 (L2)	2.84	1.2

Figure 21 compares the building PFA and PIDR responses during the service level events pre- and post-fire (i.e., tests EQ1—EQ3 and EQ8). Although the seismic demands on the building were relatively low during these service-level earthquakes, the building observed apparent acceleration attenuation effects and larger interstory drifts during the post-fire test EQ8. This is due to the fact that building sustained substantial stiffness deterioration due to the damage accumulated during the prior earthquake and fire tests. As a result, the PIDRs achieved during the post-fire service level test (test EQ8) were about twice as large as those attained during the post-fire service level test sequence (EQ1—EQ3).

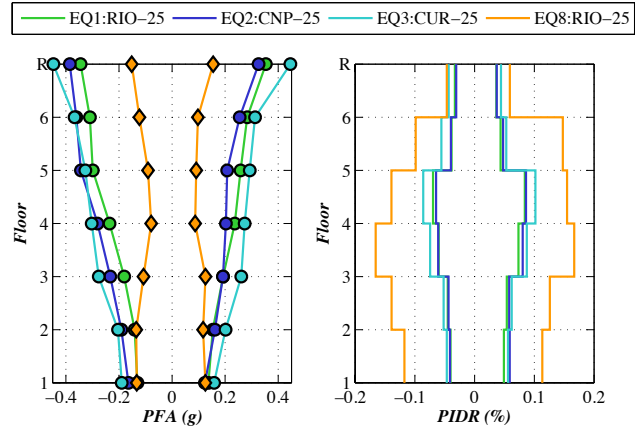


Figure 21. Building peak responses during the service level tests: (a) peak floor accelerations, and (b) peak interstory drift ratios.

In contrast, Figure 22 presents the building PFA and PIDR responses during the above-the-service-level events (i.e. tests EQ5—EQ7 and EQ9). As the motion intensity increased, the largest PIDR reached about 1.0% during the design motion (test EQ6) and above 1.5% during the MCE motion (test EQ7). It is also revealed that the largest PIDR occurred at the mid-height of building (level 3 and 4) throughout the pre-fire earthquake test sequence. These results are consistent with building physical observations. In addition, the PFA increased almost monotonically up the height of the building during the pre-fire earthquake test sequence, indicating a fundamental-mode dominant structural response in these tests. In contrast, the final earthquake test (near-fault MCE event EQ9) subjected the building to extremely large drift demands (an interstory drift ratio of above 12% at level 2) and resulted in a near-collapse condition of the specimen. It is also noted that the residual (permanent) RDR of building exceeded 1% following the test (Table 3). This is partially attributed to the fire-induced damage to the gypsum sheathing at level 2, which reduced the shear capacity of the shear walls, encouraging formation of a soft-story mechanism during the final near-fault earthquake (EQ9) at this level.

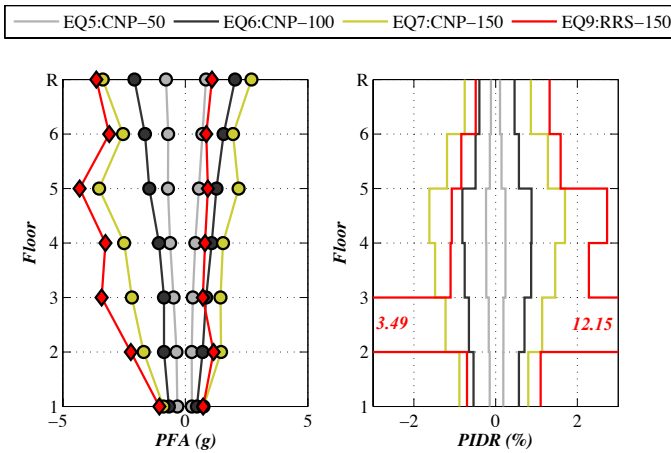


Figure 22. Building peak responses during the above-service level tests: (a) peak floor accelerations, and (b) peak interstory drift ratios.

Comparison of Floor Acceleration Amplification: Figure 23 presents the acceleration amplification factor Ω of the test building during the earthquake tests, where part a includes those scaled to service level event intensity; and part b includes the above-service level scaled motions. It is noted that a mix of pre- and post-fire tests are overlaid. The acceleration amplification factor Ω is determined as the ratio between the peak acceleration achieved at each floor and the peak acceleration of the input motion. According to ASCE 7-10 (ASCE, 2010) code provisions, the amplification factor is empirically defined as $1+2z/h$ (z/h denotes the normalized building height), which represents a linear distribution along

the building height from 1.0 at the base to 3.0 at the roof. During the pre-fire service test sequence (EQ1-EQ3) (Figure 22a), the acceleration amplification factors increased monotonically up the height of the building with the largest values ranging between 2.0 and 2.5 at the roof, which is slightly lower than the code-specified value of 3.0. In contrast, as the building sustained significant period elongation prior to the post-fire service level test EQ8, the attenuated acceleration distribution was observed along the building height ($\Omega \sim 1.0$). The amplification effects continued to increase during tests EQ5 and EQ6 as the motion intensity increased (Figure 23b). It is noted that the amplification distribution achieved during the design event (test EQ6) agrees well with the code-specified distribution along the building height. During the two MCE events (tests EQ7 and EQ9), the observed floor amplification effects were significantly larger than the code-specified distribution at all floors (Figure 23b). This may also be partially due to the presence of impulse-like acceleration spikes during these tests.

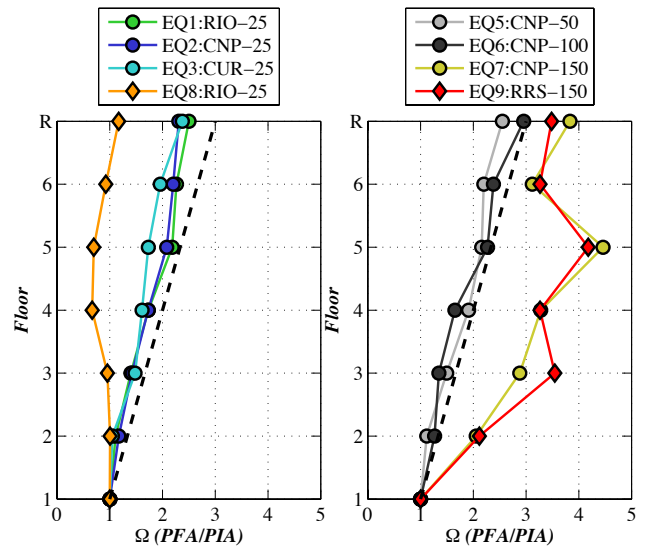


Figure 23. Acceleration amplification ratios of the test building under: (a) service level tests, and (b) above-service level tests

Physical Observations: Post-Fire Tests

Rapid inspection was conducted following the service level aftershock test (EQ8), which confirmed no observed damage to the building due to its low seismic demands (PIDR < 0.2 % and PFA < 0.2 g). The final physical inspection of test building was conducted following the completion of the near-fault extreme earthquake event (EQ9). To obtain a comprehensive understanding of the final damage of the structural components, inspection of the building interior at the final stage involved the sheathing damage documentation and subsequently the wall framing and the sheathing steel of

the structural panels by removing the compartment-side interior gypsum panels. Due to the extremely large drift demands at level 2 of the test building (transient PIDR > 12% and residual IDR ~ 6%) during EQ9, the building developed a soft-story mechanism at the completion of the extreme event test (Figure 24).



Figure 24. North exterior elevation of the test building: (a) pre-EQ9 condition, and (b) post-EQ9 condition, and (c) post-EQ9 condition at the lower three levels.

The excessive interstory drift demands are associated with severe damage to the structural components of level 2 and, importantly, revealed the ultimate damage mechanism of the lateral loading resisting system. The test building, however, resisted collapse largely due to redistribution of loads and the framing action of the continuous rod tie-down system. Despite the larger interstory drift demands, the damage to the building at all remaining levels was similar to those observed in the pre-fire test sequence. In this regard, herein the focus is on observed damage of level 2. Interested readers are referred to the technical report (Wang et al., 2017b) for additional damage documentation.

Figure 25 offers an example of the structural sheathing damage of the corridor and the four compartments. It is noted that steel sheathed panels of the corridor shear walls were located on the corridor side, while those of the corner walls were located on the exterior side. On the other hand, the building interior (compartment side) was all sheathed with

Type X gypsum panels inside of the four compartments. Sans the northeast compartment, the remaining three compartments at level 2 were subjected to fire damage prior to the extreme MCE earthquake test (EQ9).

Evident in the post-event physical inspection was the near complete tearing of a large extent of the structural sheathing, partial or full-delamination of sheathing face gypsum and associated detachment of gypsum on the opposing face. Consequently, structural components of the wall (framing members) suffered extensive global and local buckling (e.g. Figure 26).



Figure 25. Damage observed to corridor shear wall steel sheathed panels following the completion of the extreme MCE event (EQ9): (a) east corridor, (b) west corridor, (c) global buckling of steel sheathed panels, and (d) fastener pull-over failure.



Figure 26. Damage observed to Southwest corridor shear wall at level 2 following of the extreme MCE event (EQ9): (a) wall framing, (b) vertical study local buckling at the base and stud-to-track connection failure, (c) compression post local buckling at the base, (d) tie-down assembly (west side), (e) stud global buckling, and (f) uplifted bottom track at the west end of the wall.

Concluding Remarks

A substantial growth in the use of cold-formed steel (CFS) framed construction has recently been observed, notably in high seismic regions in the western United States. Structural systems of this kind consist of light-gauge framing members (e.g., studs, tracks, joists) attached with sheathing materials (e.g., wood, sheet steel). CFS-framed structures can offer lower installation and maintenance costs than other structural types, particularly when erected with prefabricated assemblies. They are also durable, formed of an inherently ductile material of consistent behavior, lightweight, and manufactured from recycled materials. Compared to other lightweight framing solutions, CFS is non-combustible, an important basic characteristic to minimize fire spread. While these lightweight systems provide the potential to support the need for resilient and sustainable housing, the state of understanding regarding their structural behavior in response to extreme events, in particular earthquakes and ensuing hazards, remains relatively limited.

To advance knowledge regarding the multi-hazard performance of mid-rise CFS construction, a full-scale six-story cold-formed steel building was constructed and tested on the UCSD Large High Performance Outdoor Shake Table test facility between April and July 2016. Within this three-week test program, the test building was first subjected to a suite of seven earthquake motions with progressively increasing motion intensity (from service to MCE level). Following the first seven earthquake tests, live fire tests were conducted on the earthquake-damage building in six strategically selected rooms to evaluate the performance of fire protection systems and the impact of seismic damage of the building and the associated characteristics of the fires that ensued. Finally, for the first time, the test building was subjected two post-fire earthquake tests, including a low-amplitude ‘aftershock’ and an extreme near-fault target MCE-scaled motion. In addition, low-amplitude white noise and ambient vibration data were collected during construction and seismic testing phases to support identification of the dynamic state of the building-NCS system.

In this paper, the test program is documented, and results from the pre- and post-earthquake tests are discussed; both in terms of measurements and importantly utilizing physical observations. Preliminary key findings from these two test phases include the following:

Pre-Fire Earthquake Tests

The test building suffered minimal damage during the service level earthquake tests and remained largely in the quasi-linear range, with very low drift demands imposed on the specimen (interstory drift < 0.2%). During the design level earthquake test, the corridor shear and gravity walls at level 3 and 4 suffered damage in the form of gypsum panel crushing and fastener withdrawal when the interstory drifts at these two levels reached about 1.0%. This is corroborated by the fact that the building fundamental period increased by more than 50%. Damage continued to progress as the interstory drift exceeded 1.5% during the maximum considered earthquake (MCE) test, however observed damage to the building remained readily repairable, with the structural shearwalls at the lower floors (those that could be inspected) developing their intended local steel sheathing buckling mechanism near attachment points along framing member perimeters. The building structural components performed satisfactorily throughout the pre-fire earthquake test sequence. The most significant damage to the structural system, as noted, occurred in the form of buckled sheet steel on the corridor shear walls composite panels.

Post-Fire Earthquake Tests

The low-amplitude aftershock induced following the fire tests significantly attenuated seismic demands in the building as a result of the elongated period caused by the pre-fire earthquake sequence. In contrast, the extreme near-fault earthquake test (EQ9) developed a full soft story mechanism at level 2 and caused severe damage to the buildings structural system (complete loss of structural integrity of corridor and exterior longitudinal shear walls). It is highly laudable that the test building resisted collapse due to redistribution of loads and framing action of the building rod tie-down system.

Acknowledgements

This project is a collaboration between two academic institutions (University of California, San Diego and Worcester Polytechnic Institute), two government or institutional granting agencies (Department of Housing and Urban Development and the California Seismic Safety Commission) and more than fifteen industry partners. It is noted that although UCSD led the overall test program, this team's primary focus was on the earthquake testing phases, while WPI's primary focus was on the fire testing phases. We also thank the Jacobs School of Engineering and Department of Structural Engineering at UCSD for matching support of this effort. Industry sponsors include the California Expanded Metal Products Co. (CEMCO) and Sure-Board, who each provided financial, construction, and materials support. Specific individuals that dedicated significant time on behalf of this effort included Fernando Sesma (CEMCO), Kelly Holcomb, Carleton Elliot and Tyler Elliot (Sure-Board), Harry Jones (DCI Engineers), Diego Rivera (SWS Panels), Doug Antuma (Rivante), Larry Stevig (State Farm Insurance), Tim Reinhold and Warner Chang (Insurance Institute for Business and Home Safety), Steve Helland (DPR Construction), Rick Calhoun (Walters & Wolf), and Jesse Karnes (MiTek). We appreciate the efforts of these individuals and their colleagues at their respective firms.

Regarding support for the test program, the efforts of of NHERI@UCSD staff, namely, Robert Beckley, Jeremy Fitcher, Dan Radulescu, and Alex Sherman, are greatly appreciated. The authors are also grateful to Professor Yehuda Bock and graduate student Dara Goldberg from the Scripps Institute of Oceanography at UCSD for providing the Global Positioning System and related technical support, and Professor Falko Kuester and his students from the Department of Structural Engineering at UCSD for collecting aerial video footage and LiDAR image data of the test specimen. Experiments performed at the National Institute of Standards and Technology (NIST), led by Dr. Matthew Hoehler, supported the planning of this test program, are

greatly appreciated. In addition, the authors also greatly appreciate UCSD Department of Environment, Health & Safety, and the San Diego Fire Department for providing the necessary approvals and fire department participation during the fire-testing phase of this effort. The above continuous support is gratefully acknowledged. Findings, opinions, and conclusions are those of the authors and do not necessarily reflect those of the sponsoring organizations.

References

- AISI (American Iron and Steel Institute) (2007). *North American standard for cold-formed steel framing—Lateral design*. AISI S213, Washington DC.
- AISI (American Iron and Steel Institute) (2012). *North American specification for the design of cold-formed steel structural members*. AISI S100, Washington DC.
- Al-Kharat, M., and Rogers, C. A. (2007). "Inelastic performance of cold-formed steel strap braced walls." *J. Constr. Steel Res.*, 63(4), 460–474.
- ASCE (American Society of Civil Engineers) (2010). *Minimum Design Loads for Buildings and Other Structures*. ASCE 7, Reston, VA
- Balh, N., DaBreo, J., Ong-Tone, C., El-Saloussy, K., Yu, C., and Rogers, C. A. (2014). "Design of steel sheathed cold-formed steel framed shear walls." *Thin-Walled Struct.*, 75, 76–86.
- Branston, A., Chen, Y. C., Boudreault, F. A., and Rogers, C. A. (2006). "Testing of light-gauge steel-frame—Wood structural panel shear walls." *Can. J. Civ. Eng.*, 33(5), 561–572.
- Fiorino, L., Della Corte, G., and Landolfo, R. (2007). "Experimental tests on typical screw connections for cold-formed steel housing." *Eng. Struct.*, 29(8), 1761–1773.
- Fülöp, L. A., and Dubina, D. (2004). "Performance of wall-stud cold-formed shear panels under monotonic and cyclic loading. Part I: Experimental research." *Thin-Walled Struct.*, 42 (2), 321–338.
- Landolfo, R., Fiorino, L., and Della Corte, G. (2006). "Seismic behavior of sheathed cold-formed structures: Physical tests." *J. Struct. Eng.*, 132(4), 570–581.
- Liu, P., Peterman, K.D., and Schafer, B.W. (2014). "Impact of construction details on OSB-sheathed cold-formed steel framed shear walls." *J. Constr. Steel Res.*, 101, 114–123.

Nithyadharan, M., and Kalyanaraman, V. (2013). "Modelling hysteretic behaviour of cold-formed steel wall panels." *Eng. Struct.*, 46, 643-652.

Peterman, K.D., Stehman, M.J., Madsen, R.L., Buonopane, S.G., Nakata, N., and Schafer, B.W. (2016a). "Experimental seismic response of a full-scale cold-formed steel-framed building. I: System-level response." *J. Struct. Eng.*, 04016127.

Peterman, K.D., Stehman, M.J., Madsen, R.L., Buonopane, S.G., Nakata, N., and Schafer, B.W. (2016b). "Experimental seismic response of a full-scale cold-formed steel-framed building. II: Subsystem-level response." *J. Struct. Eng.*, 04016128.

Serrette, R., Encalada, J., Juadines, M., and Nguyen, H. (1997). "Static racking behavior of plywood, OSB, gypsum, and fiberboard walls with metal framing." *J. Struct. Eng.*, 123(8), 1079–1086.

Shamim, I., Dabreo, J., and Rogers, C.A. (2013). "Dynamic testing of single- and double-story steel-sheathed cold-formed steel-framed shear walls." *J. Struct. Eng.*, 139(5), 807–817.

Wang, X., Hutchinson, T.C., Hegemeir, G., Gunisetty, S., Kamath, P., and Meacham, B. (2017a). Earthquake and post-earthquake fire performance of a mid-rise cold-formed steel framed building - test program and test results: Final Report (CFS Test Program Report #2). Structural Systems Research Project. Report No. SSRP-16/08. University of California, San Diego. La Jolla, CA.

Wang, X., Hutchinson, T.C., Hegemeir, G., and Gunisetty, S. (2017b). Earthquake and post-earthquake fire performance of a mid-rise cold-formed steel framed building - supplemental materials: Final Report (CFS Test Program Report #3). Structural Systems Research Project. Report No. SSRP-16/09. University of California, San Diego. La Jolla, CA.

Yu, C. (2010). "Shear resistance of cold-formed steel framed shear walls with 0.686 mm, 0.762 mm, and 0.838 mm steel sheet sheathing." *Eng. Struct.*, 32 (6), 1522–1529.